Engineering Geology 224 (2017) 1–14

Contents lists available at ScienceDirect

Engineering Geology

journal homepage: www.elsevier.com/locate/enggeo

Reconstructed seismic and tsunami scenarios of the 1905 Calabria earthquake (SE Tyrrhenian sea) as a tool for geohazard assessment

M.F. Loreto[a,*], G. Pagnoni[b], F. Pettenati[c], A. Armigliato[b], S. Tinti[b], D. Sandron[c], F. Brutto[d], F. Muto[d], L. Facchin[c], F. Zgur[c]

[a] Institute of Marine Sciences, CNR, Bologna, Italy
[b] Dipartimento di Fisica e Astronomia (DIFA), Univ. of Bologna, Italy
[c] Istituto Nazionale di Oceanografia e di Geofisica Sperimentale (OGS), Sgonico, Trieste, Italy
[d] Dipartimento di Biologia, Ecologia e Scienze della Terra (DiBEST), Univ. of Calabria, Arcavacata di Rende, CS, Italy

ARTICLE INFO

Keywords:
Active tectonics
KF-scenarios
Tsunami scenario
Environmental effects
Risk analysis
1905 Calabria earthquake

ABSTRACT

Italy is one of the most seismically active regions in the central Mediterranean and one of the countries with the longest record of historical earthquakes in the world. Over the last decades the scientific community has recognised the value of historical data when used to constrain modelling tools in hazard analyses. This is the case of the destructive 1905 Calabria (South Italy) earthquake, followed by a tsunami and by many secondary effects on the environment observed both inland and offshore. Recently acquired geophysical data allowed to identify an active normal fault, named Sant'Eufemia Fault, located nearshore in the Sant'Eufemia Gulf (SE Tyrrhenian sea), considered the most probable seismogenic source of the 1905 earthquake and capable to trigger future events.

In this paper we perform a scenario-based deterministic analysis for an earthquake resulting from the rupture of the Sant'Eufemia fault (SEF) and a preliminary potential risk analysis. After defining source parameters compatible with the 1905 earthquake (ca. 40 km fault length and ca. 2.3 m slip, Mw 6.9), KF-analysis and tsunami simulations are carried out and modelling results are compared against historical available data. The obtained results allow one to border areas in central Calabria that are most exposed to geohazard deriving from the analyzed fault. Some of these areas happen to be zones with intense economic/touristic and urban development, which calls for the need to integrate the ongoing development plans with adequate programs of risk mitigation and prevention.

1. Introduction

The Mediterranean region is characterized by active geodynamic processes, responsible for the high seismicity level affecting the active arc systems (Fig. 1, top). In the Central Mediterranean, the Calabrian Arc system exhibits the highest release of seismic moment in terms of historical (see Fig. 1b; Rovida et al., 2011) and of instrumental seismicity (see Fig. 1a; http://www.seismicportal.eu/; see also http://csi.rm.ingv.it/versione_inglese/index_eng.htm; Castello et al., 2004; Chiarabba et al., 2005; CSTI 1.0 Working Group, 2001). It follows that this region is affected by the highest hazard and risk level of the Central Mediterranean area, linked both to earthquakes and tsunamis (Tinti, 1993; Slejko et al., 1998; Lucantoni et al., 2001; Tinti and Armigliato, 2003; Gruppo di Lavoro MPS, 2004). Moreover, tsunamis were triggered by several of the largest earthquakes that struck the Central Mediterranean (Tinti and Maramai, 1996; Tinti et al., 2004; Maramai et al., 2014). Restricting the attention to Calabria and eastern Sicily (Fig. 1c), examples of these earthquake-generated tsunamis are the well-known occurrences of 1693 in eastern Sicily (e.g. Tinti et al., 2001), of 1783 in central-southern Calabria (e.g. Tinti and Gavagni, 1995), of 1905 in western Calabria (Tinti and Piatanesi, 2002) and of 1908 in the Messina Straits (Tinti and Armigliato, 2001). Several studies have been performed by the scientific community during the last decades to identify the source faults capable to generate these earthquakes. A good synthesis of the research carried out until today can be found in the freely accessible database DISS showing the active seismogenic faults of Italy (DISS: http://diss.rm.ingv.it/dissmap/), in which the recently identified (Loreto et al., 2013) fault source of the 1905 is included (Fig. 1d). Looking at the DISS faults map, one can observe that the Calabria and NE-Sicily regions are the ones with the largest, and well assessed, NE-trending seismogenic sources (Fig. 1d), such as the ones involved in the 1783 and 1908 events and the one that

* Corresponding author.
E-mail address: filomena.loreto@bo.ismar.cnr.it (M.F. Loreto).

http://dx.doi.org/10.1016/j.enggeo.2017.04.018
Received 28 November 2016; Received in revised form 23 March 2017; Accepted 16 April 2017
Available online 27 April 2017

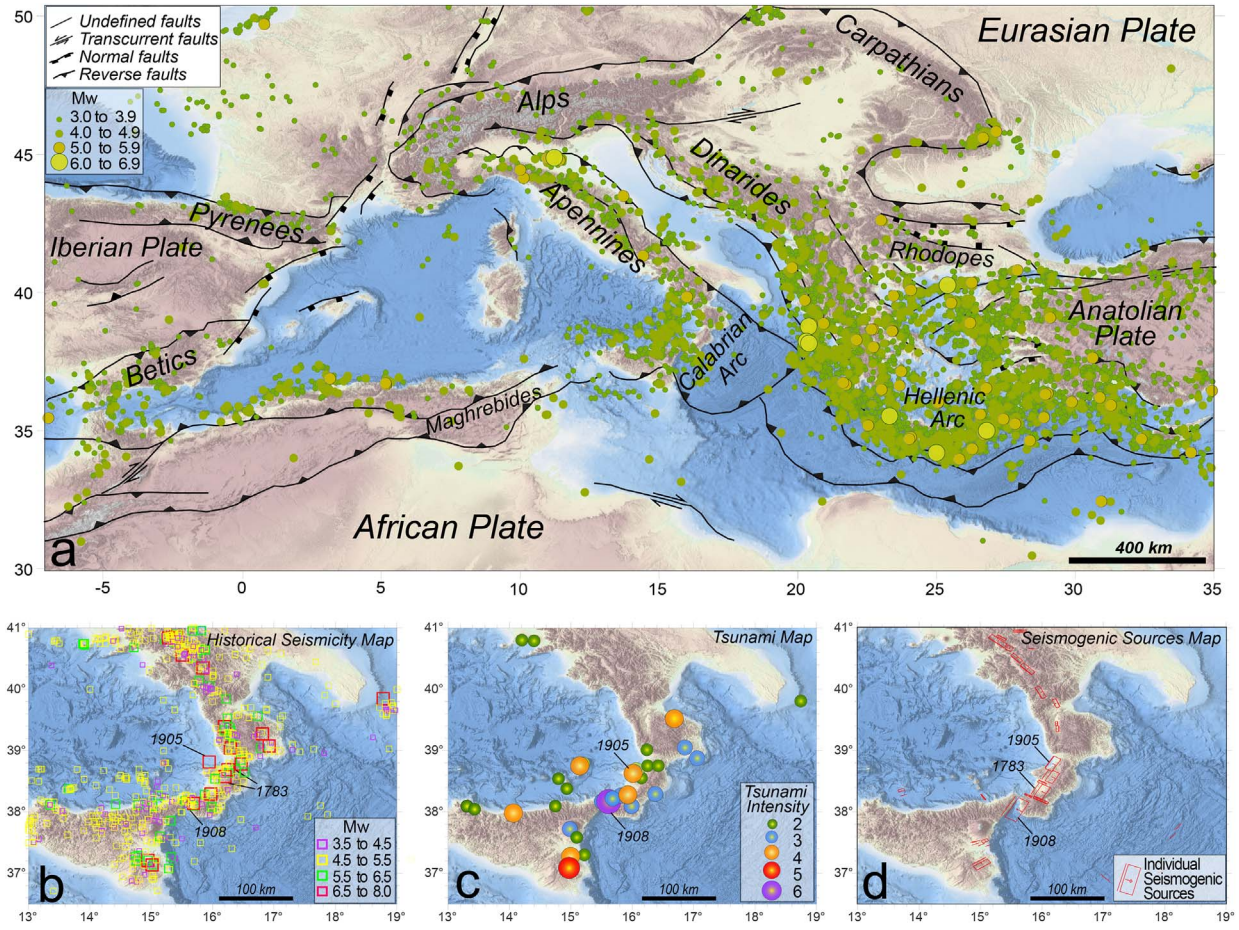

Fig. 1. Shaded relief from EMODnet bathymetry portal (http://portal.emodnet-bathymetry.eu/gebco-bathymetry-basemap). a) Mediterranean structural sketch modified after an online Tectonic Map (Woudloper - Own work, CC BY-SA 1.0). Instrumental seismicity (2012–2013) from EMSC (http://www.seismicportal.eu/). b) Historical Seismicity Map (1000–2006) from INGV seismic database (Rovida et al., 2011). c) Tsunami Map modified after Maramai et al. (2014): tsunami intensity is expressed in the Sieberg-Ambraseys scale. d) Seismogenic Sources Map, including only individual sources, modified after DISS (http://diss.rm.ingv.it/dissmap/dissmap.phtml). Marked are the most important historical events that struck the region.

can be associated with the 1905 event.

The aim of this work is to reconstruct the 1905 event that hit western-central Calabria by modelling an integrated scenario including the macroseismic field, the impact of tsunami on the coast and the environmental effects. The motivation of this study is that the source fault of this earthquake, which is one of the largest occurred in Calabria in the last centuries, was and is still object of a debate where many authors propose different parent faults. The scenario elaborated here takes the recently identified Sant'Eufemia fault (SEF; Loreto et al., 2013; Sandron et al., 2015) as the fault responsible for the earthquake. The good comparison between the observations and modelling results can be used as a validation of the source fault hypothesis. It is also stressed that this study provides a contribution to assessing seismic and tsunami hazard for Calabria. A relevant outcome is that the computed 1905 integrated scenario shows that several zones, currently characterized by development of infrastructure facilities and tourism activities fall within the high-impact region of the 1905 event, which outlines the need for developing appropriate, now missing or insufficient, mitigation plans.

2. Geo-structural setting

The Sant'Eufemia Gulf (Fig. 2) lies between the Calabrian Arc and the southeastern side of the Tyrrhenian basin, a Neogene-Quaternary back-arc basin belonging to the Apennines-Ionian crust subduction system (Patacca and Scandone, 2004). The Calabrian Arc is an independent, continental block that bridges the NW-trending southern Apennines (to north) with the approximately E-trending Sicilian Apennines (to south; Bonardi et al., 2001; Critelli et al., 2017). The rapid southeast-ward migration of the Calabrian Arc, and the abundant seismicity recorded at different depths support the hypothesis that subduction of the oceanic crust is still active beneath the Calabrian block. Laterally, the subduction is confined by two main tear faults: the well identified Tindari fault to south; and the Sangineto-Crati faults system (Van Dijk and Scheepers, 1995; Rosenbaum et al., 2008) or the Catanzaro shear zone (Guarnieri, 2006; Brutto et al., 2016) to north. The Calabrian Arc is further segmented, laterally, by NW-trending shear zones that, from middle Miocene (Van Dijk and Scheepers, 1995) to Recent (Tansi et al., 2007; Tripodi et al., 2013), have accommodated differential movements between minor blocks (Malinverno and Ryan, 1986). Further, this transversal system allowed the opening of Neogene transversal basins like that hosted in the Catanzaro paleo-strait (Ghisetti, 1979; Zecchin et al., 2015). From middle Pleistocene times, the Calabrian Arc experienced a rapid uplift up to ~1 mm/yr (Westaway, 1993; Tortorici et al., 2003), partially accommodated by the major NE-trending normal faults (Ghisetti, 1979; Monaco and Tortorici, 2000; Brutto et al., 2016) affecting the entire Calabria block. These NE-trending normal faults, all active, are arranged as graben and semi-graben systems, such as the Crati graben or the more recently defined Lamezia graben (Brutto et al., 2016). Most of these active normal faults are associated to the largest historical earthquakes that struck the region (Figs. 1b and 2).

3. The 1905 Calabria earthquake and tsunami

The earthquake that in the night of 8th September 1905 hit the

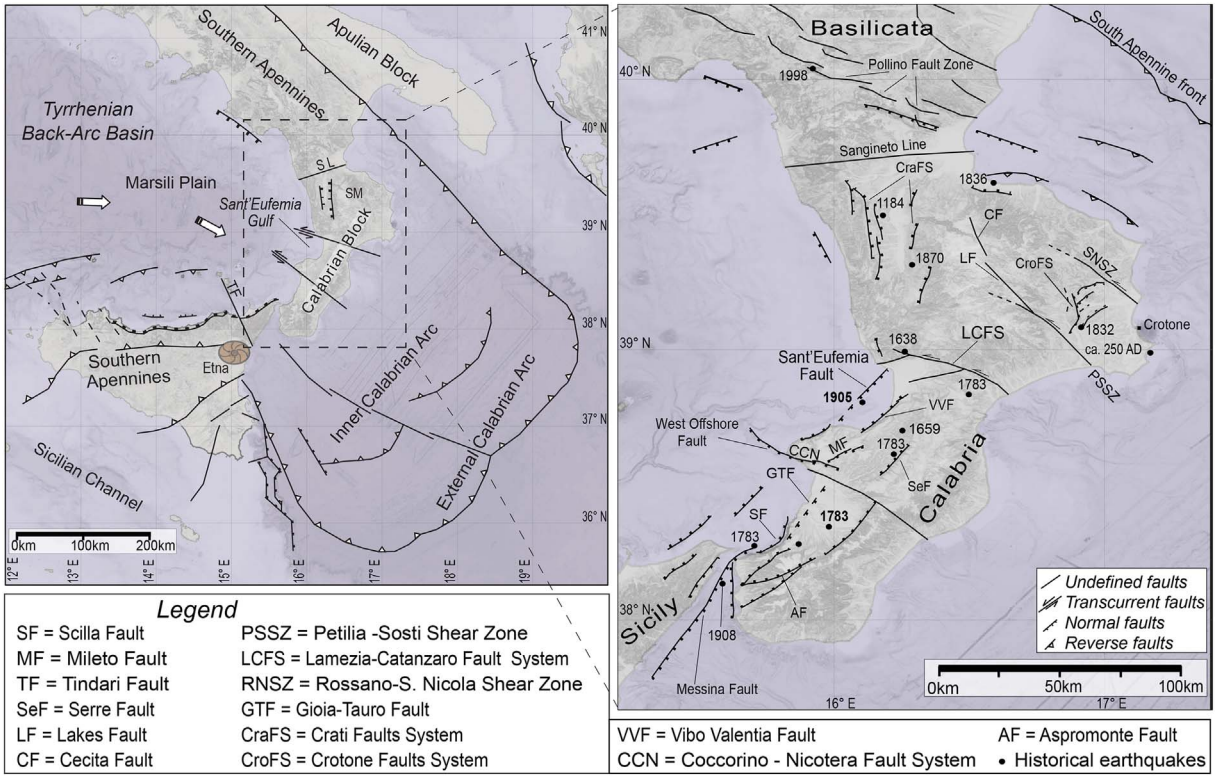

Fig. 2. Structural setting adapted from Barone et al. (1983), Tortorici et al. (1995), Polonia et al. (2011), Galli et al. (2010), Pepe et al. (2013), Loreto et al. (2013), Brutto et al. (2016). Topo-bathymetry from the EMODnet data (http://portal.emodnet-bathymetry.eu/) and from the 90-m resolution SRTM (Jarvis et al., 2008). Left: Sketch of the Southern Apennines system. Right: Detail of the main tectonic features (active faults, physiographic elements, and historical earthquakes with Mw > 6.5).

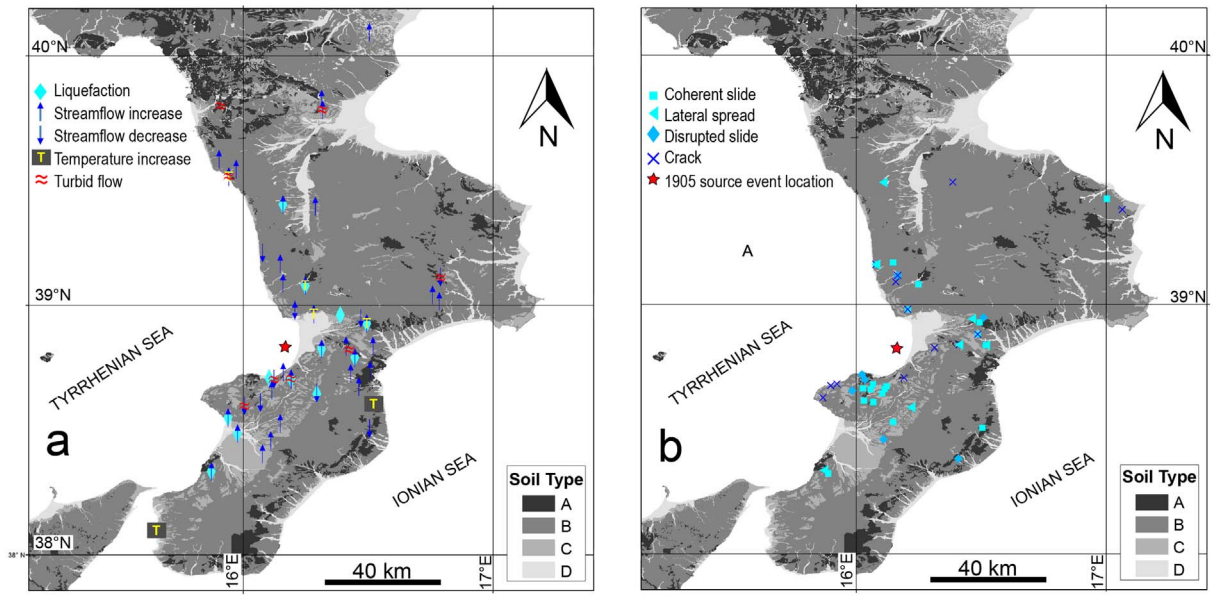

Fig. 3. Environmental effects associated to the Calabria 1905 earthquake (Rizzo, 1907) plotted on a soil-type map: type A (bedrock); type B (soft rocks, stiff deposits); type C (tight, coarse and fine deposits); and type D (loose, coarse and fine deposits), according to the lithological classification by Di Capua et al. (2011a and b). a) Map of hydraulic effects; b) Map of instability phenomena.

central-western Calabria region caused > 550 victims and about 2000 injured people (Baratta, 1906), triggering also a tsunami that, though feeble, was observed both offshore and along the coast (e.g. Tinti and Maramai, 1996; Tinti et al., 2004). Coeval documents (Rizzo, 1907; Platania, 1907) list numerous environmental effects observed by people in a widespread area of the Calabria region and offshore. These effects are mainly represented by: changing in the water flow and in the temperature of rivers and springs; turbid flow and liquefaction seen immediately after the earthquake; diffuse ground cracking, coherent and disrupted landslides and lateral spreading. We plot all environmental effects, using a well-organized database (see Tertulliani and Cucci, 2009), in two separate maps grouping all hydraulic effects such as liquefaction, stream-flow variation, fluid temperature variation and turbidity (Fig. 3a), and instability phenomena such as coherent and disrupted slides, cracks and lateral spreadings (Fig. 3b).

The observations related to the tsunami consist of 1) recordings of

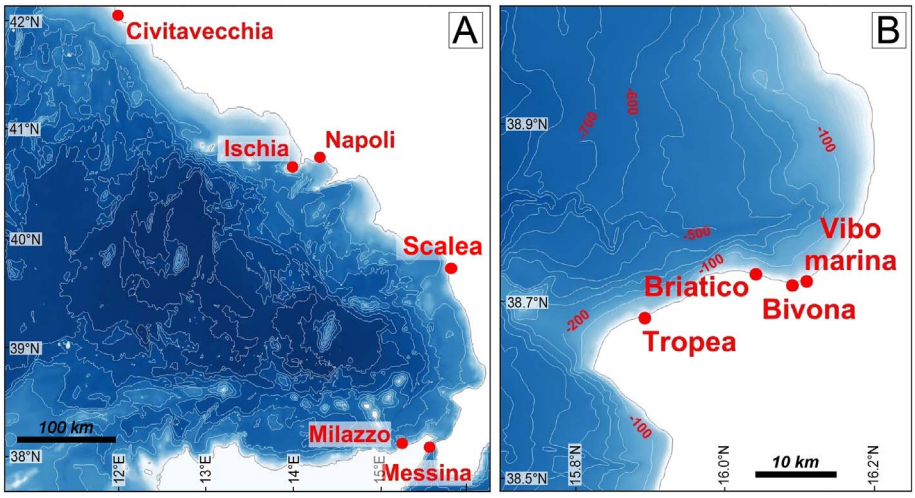

Fig. 4. A) Map of the tide gauges that recorded the 1905 tsunami (Civitavecchia, Ischia, Naples and Messina) and/or for which port authority observations are reported (Milazzo). B) Map of the sites in the near-field where observations are available (see Table 1). Bathymetry is produced by gridding data from ISTEGE project 2010 and an older dataset provided by the former CNR - Istituto di Geologia Marina (now ISMAR) in Bologna.

some tide gauge stations located in the intermediate and far field along the Tyrrhenian coastlines, and 2) accounts by eyewitnesses, collected and critically revised in several coeval and later reports and studies.

Regarding the tide gauge data, a report by Platania (1907) provides useful details on wave characteristics measured at the stations of Messina (Sicily), Naples and Ischia (Campania), Civitavecchia (Latium; see Fig. 4). Unfortunately, the instrument located closest to the source area (Messina) started recording only about 6 h and 40 min after the mainshock, depriving us of very precious information on the arrival time.

Tsunami coastal effects were described, though very succinctly, by several authors in coeval reports and studies (Baratta, 1906; Mercalli, 1906; Rizzo, 1906; Platania, 1907), as may be found in the catalogue of the Italian tsunamis (Tinti et al., 2004). At Bivona, nowadays a suburb of Vibo Valentia (Fig. 4b), the sea rose suddenly and penetrated for about 30 m on the beach, carrying a boat onshore. At Vibo Marina (called Porto Santa Venere in 1905), the sea inundated the beach for about 6 m, carrying several boats that were left onshore when the sea withdrew. At Briatico, a boat, laid at anchor, was pushed 7–8 m on land and the sea brought numerous dead fish on the beach. At Tropea, the sea rose suddenly by about 2 m and 5 boats placed on the beach were carried out to the sea.

Tsunami effects were observed also far away from the source zone, especially at Scalea (Fig. 4a), where the sea, initially very quiet, invaded the beach for > 30 m, carrying and pouring out several boats laying on the shore. In this location, only one report by Rizzo (1906) mentions an observed height of 6 m. In Sicily, the harbour office of Milazzo referred that the sea rose and lowered every 30 min with an amplitude of 80 cm. We summarize all these observations in Table 1. Furthermore, there are accounts by sailors and fishermen who heard and saw anomalies related to the tsunami waves off Bivona, and in the sea between Milazzo, the Aeolian Islands and Calabria. Moreover, a submarine telegraph cable that connected the Aeolian islands to Milazzo, was broken during that night at about 1180 m depth.

4. Data

This study is based on the analysis of onland geological data, offshore geophysical data, historical observations that together are used to constrain the seismological and tsunamigenic modelling and to verify the results.

4.1. Structural data

The onland survey was focused on the western margin of the Catanzaro trough. The wide structural dataset, collected in the frame of a PhD project by Brutto (2016), has been analyzed in order to define the geometric arrangement of faults and the Quaternary stress field of the whole study area. Among these data, we selected a set of measurements of faults that offset the Middle-Upper Pleistocene deposits close to the Lamezia-Catanzaro fault system (LCFS in Fig. 2; and white square in Fig. 5b).

4.2. Geophysical and morphological data

We analyzed submarine high resolution morpho-bathymetric (HRMB) data and sub-bottom profiles (SBP), acquired in the frame of the ISTEGE project during the summer 2010 aboard of the R/V OGS-Explora (Loreto et al., 2012), together with middle and high resolution onland morphological data.

SBP were acquired using a Benthos CAP-6600, consisting of 16 keel mounted transducers. Sweep ranged between 2 and 7 kHz, with the resulting configuration ensuring a full ocean depth investigation. Chirp data imaged in detail the uppermost section of the sedimentary cover down to ca. 75 m depth, assuming a constant 1550 m/s sound speed within shallowest sediments.

HRMB data were acquired using two hull mounted multibeam echosounders, a Reson Seabat 8111 (100 kHz) and 8150 (12 kHz). The Seabat 8111 was employed up to 400 m depth (maximum swath width of 7.4 times the water depth), the Seabat 8150 was employed for water depth > 500 m (maximum swath width of 4.5 times the water depth), and both echosounders for the 400–500 m depth range. Processed data are gridded at different cells size and the best resolution in a shallow water depth is a grid cell size of 5 × 5 m.

Onland high resolution DEM data (10 m) were collected between 2000 and 2015 by students in the frame of graduate and PhD works, gathered and harmonized by Brutto (2016) in the frame of his PhD thesis. These data are used together with the ALOS World 3D-30 m resolution data (freely downloaded from http://www.eorc.jaxa.jp/, © JAXA).

4.3. Updating the fault geometry

Based on the only geophysical data acquired offshore, Loreto et al. (2013) defined the SE-dipping, 25 km-long Sant'Eufemia normal fault (SEF). Revisiting all available data, we move from the center of the gulf

Table 1
Summary of the available historical observations/measurements of the tsunami.

Inundation	Location	Observed penetration [m]	Period [min]	Estimated elevation [m]	
	Bivona	30		1–2	
	Briatico	8		0.5–1	
	Briatico Lido	7–8		0.5–1	
	Porto Santa Venere (Vibo Marina)	6		0.3–0.5	
	Scalea	30		1–2	
Run-up		Observed height [m]			
	Tropea	2		2	
Tide-gauge records		Peak-to-peak height [m]	Period [min]		Polarity of the first arrival
	Messina[a]	0.10	7–8	0.05–0.10	Not available
	Napoli Mandracchio[b]	0.03	11	?	Not available
	Napoli Arsenale	0.18	10	?	Negative
	Ischia	0.12	12	?	Negative
	Civitavecchia	0.07	8	0.05–0.10	Negative

[a] The instrument begun to register only after 9:20 am, that is approximately six hours and forty minutes after the mainshock.
[b] Doubtful registration, the instrument was not working correctly in the night of the earthquake.

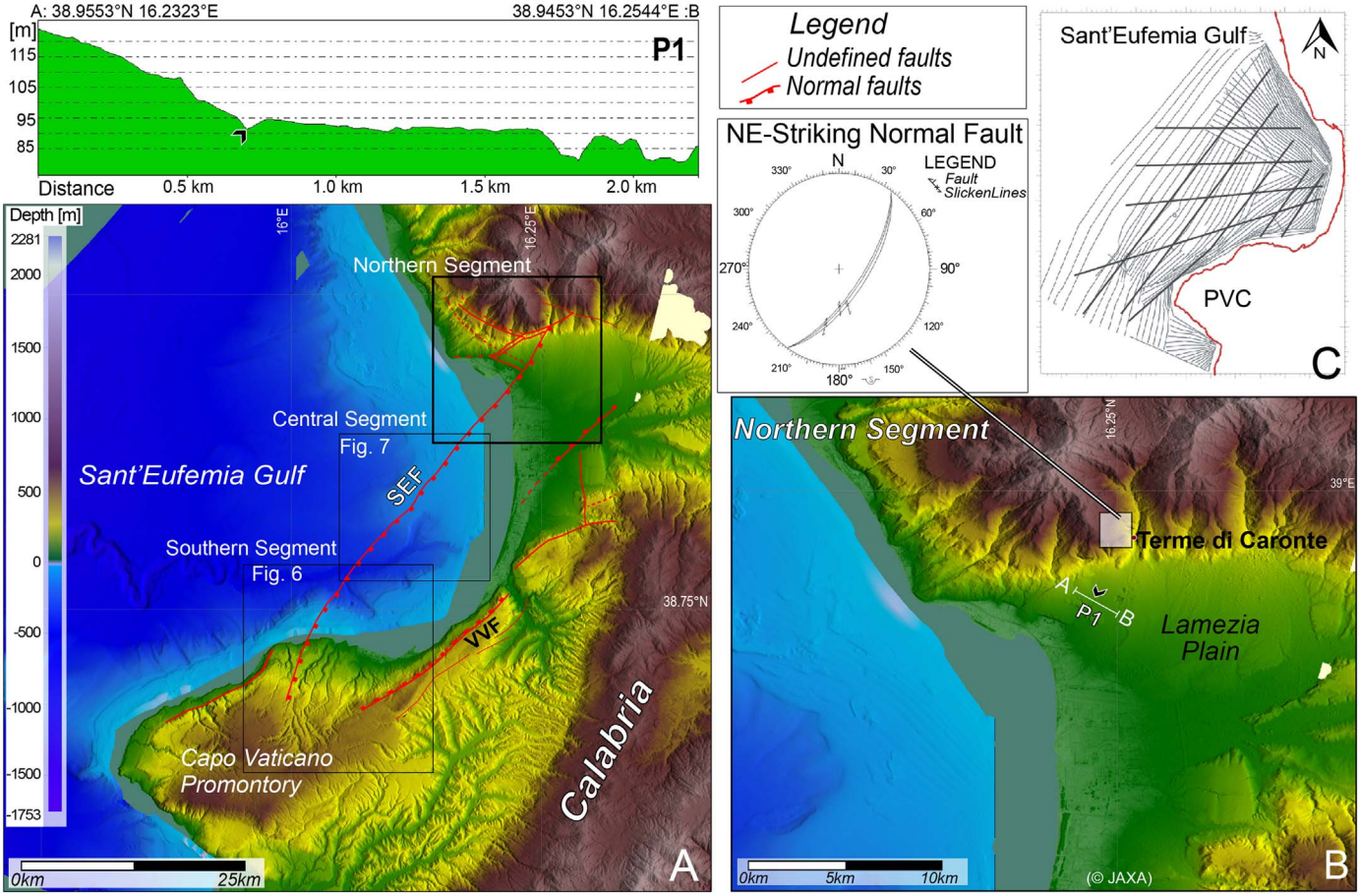

Fig. 5. A) High-resolution morpho-structural map of the study area done by combining bathymetric data acquired in the frame of the ISTEGE project (Loreto et al., 2012) and on land ALOS World 3D-30 m (http://www.eorc.jaxa.jp/, © JAXA). Faults are modified after Loreto et al. (2013) and Brutto et al. (2016). SEF: Sant'Eufemia Fault; VVF: Vibo Valentia Fault. B) Detail of northern segment showing the geo-structural measurements station (white square) close to "Terme di Caronte" locality and the altimetry profile (P1) location, this last extracted from ALOS World 3D-30 m. The inset shows the stereographic plot of NE-striking fault planes. P1: Profile 1, black dart marks the groove. C) Sketch map of the entire offshore geophysical dataset acquired in the frame of the ISTEGE project 2010.

to the north and to the south looking on land for further clues that allow us to extend laterally the fault plane (Fig. 5a).

We divided the area including the SEF into three main segments: northern, central and southern segment (Fig. 5a). In the northern segment, within Pleistocene deposits cropping out close to the "Terme di Caronte" locality, Brutto (2016) measured a set of SE-dipping, NE-striking normal faults (Fig. 5b). Unluckily, between this locality and the shoreline, thick and wide telescopically arranged alluvial fans cover the Lower-Middle Pleistocene deposits. Inspite of this, a small NE-striking groove (black arrows; Fig. 5b) oriented parallel to the NE-striking fault affects the Pleistocene deposits and alluvial fans, as confirmed by the P1 altimetry profile.

In the southern segment the analysis of reprocessed morpho-bathymetry revealed the presence of a NE-trending scarp, dipping > 8°, obliquely oriented with respect to the slope (Fig. 6a). The scarp is 3.6 km long with maximum 26.5 m of bathymetric jump (CH_25; Fig. 6b), organized in two minor, perfectly aligned segments. Even though the scarp is clearly visible in the chirp profile, the low energy

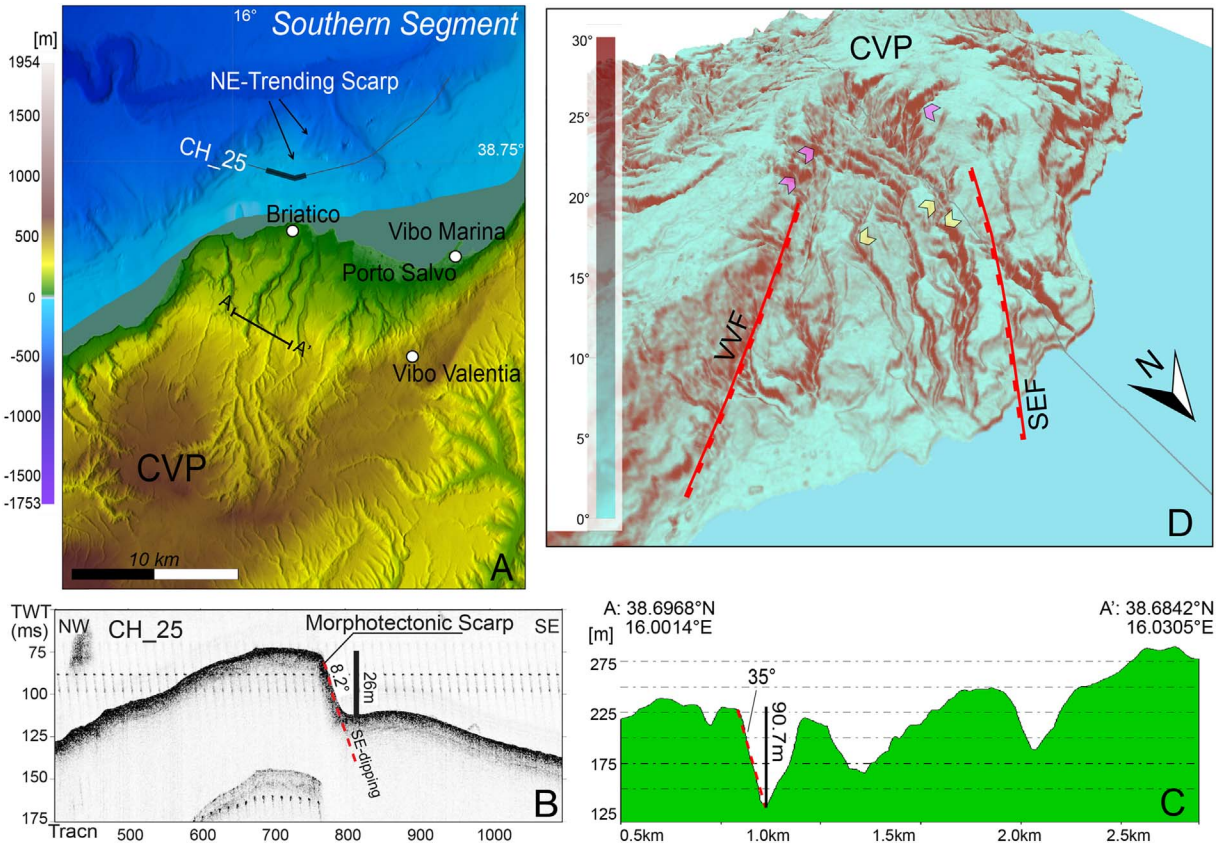

Fig. 6. A) Detail of the SEF southern segment, see Fig. 5 for location, including the navigation of CH_25 chirp profile (thin grey line), and the altimeter profile (white line) locations (A-A′); CVP: Capo Vaticano Promontory. B) Image of CH_25 chirp profile (part of a large ISTEGE 2010 dataset). C) Altimetry profile derived from ALOS World 3D-30 m data (http://www.eorc.jaxa.jp/, © JAXA). D) Slope gradient map of CVP; yellow darts mark the 90°-curved river; pink darts mark elbow river captures. Both Vibo Valentia fault (VVF) and Sant'Eufemia fault (SEF) are indicated. (For interpretation of the references to colour in this figure legend, the reader is referred to the web version of this article.)

penetration does not allow to detect sediments stratification and, thus, dislocation attributable to the fault. On land, the terrains of the northern part of the Capo Vaticano Promontory (CVP) are severely incised by channels and rivers associated with slopes up to 35° dip, visible on the slope terrain map (Fig. 6c), and with an about 70 m–altimetric jump measured in the river bed axis (A-A′; Figs. 6a and c). In this area three main rivers suddenly change flow direction, from NE to NW, resulting thus in a near 90° river curve (yellow darts; Fig. 6d). Following Howard (1967) classification, these channels are organized in a parallel/sub-parallel drainage pattern to which a geological/tectonic control can be associated. Three elbow river captures can also be identified (pink darts; Fig. 6d), that can be tectonically-controlled as already observed in other drainage basin systems (Cox, 1994; Almeida-Filho & Miranda, 2007). Based on these observations, we hypothesize that the SEF affects also part of the CVP, which is packaged between two main normal faults, the VVF and the SEF (Fig. 6d).

The central part of the high-resolution morpho-bathymetry shows a well-defined SEF plane (Fig. 7) that we used to estimate the slip amount, assuming that this scarp was generated by a unique event, namely the 1905 earthquake. We used 10 bathymetric profiles orthogonal to the fault plane in order to quantify the slip (Table 2). We decided that the fault-controlled scarp is represented by the steepest part excluding the current deep-water erosion (CE; Fig. 7). Indeed, high-resolution bathymetry shows a clear channel erosion morphology running parallel to the fault scarp (detail in Fig. 7), suggesting that the fault scarp itself acted as a barrier for downslope water flow. Among the several extracted profiles, from P1 to P10, we chose P3 as representative of channel erosion and estimated its intensity, resulting in 14.5%. We subtracted this percentage from all measured slip values (Table 2). Slip magnitudes were easily measurable on the northern part from P1 to P5, whereas it was less clear on the southern part. Therefore, here we identified as slip the highest altimetry jump among two successive depth points (see as example the P9 profile in Fig. 7; Table 2). The average slip magnitude estimated by using the values measured on bathymetry profiles is 2.3 m. Finally, the SE-ward dipping of the SEF, estimated on seismic profile GSE_07 (see in Loreto et al., 2013), is increased up to 50° considering the obliquity ($\alpha = 42°$) of the seismic profile with respect to the fault direction (Fig. 7).

According to the inland data and observations we can extend the SEF northward and southward up to about 40 km-length (Fig. 5a). Such a length is in agreement with all other NE-trending normal fault planes segmenting Calabria (Tortorici et al., 1995), and with the most credible fault source proposed by Valensise and Pantosti (2001) and Loreto et al. (2012). Using Wells and Coppersmith (1994) scale formulas we estimated a maximum fault plane width of ca. 17 km and a magnitude (Mw) of 6.9 which coincides with magnitude values found in the literature for the 1905 earthquake (Martini and Scarpa, 1982; Rovida et al., 2016). Further, we stress that the estimated slip of 2.3 m is compatible with Wells and Coppersmith (1994) formulas, according to which the average and maximum displacements for this fault size are respectively 0.99 m and 2.75 m. The focal data derived here have been used to perform tsunami modelling and KF computations.

5. Methods

Determination of the hazard characterizing the Calabria region and the surrounding is performed by using seismological and tsunami models constrained with the historical observations.

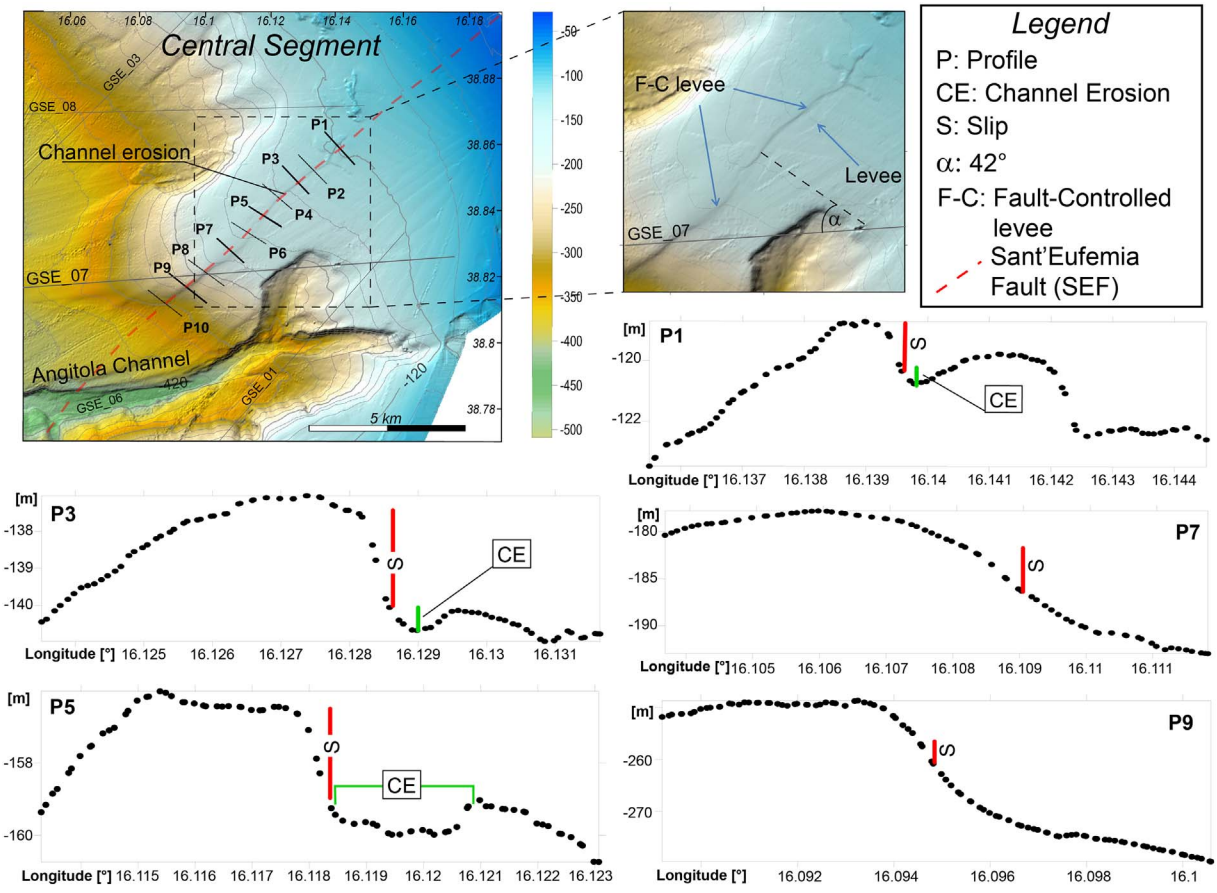

Fig. 7. High-resolution bathymetry map of the central segment including the location of bathymetric profiles, named from P1 to P10, extracted from grid data. Below we plot five of them, selected in order to represent the trend of the outcropping fault scarp. GSE_07 is the multichannel seismic profile showing the normal fault. α is the angle between the fault direction and the GSE_07 profile direction.

5.1. Tsunami modelling technique

In order to quantify the hazard due to the impact of tsunami waves along the western coasts of Calabria, we performed the tsunami propagation and inundation modelling for the Sant'Eufemia fault by means of the numerical code called UBO-TSUFD, developed and maintained by the Tsunami Research Team at the University of Bologna (Tinti and Tonini, 2013). UBO-TSUFD can solve both the linear and non-linear versions of the Navier-Stokes equations in the shallow water approximation through a finite-differences numerical scheme. The linear equations have been solved to study the regional propagation and maximum elevations distribution over a geographical domain covering the Tyrrhenian coasts of Calabria, the northern Sicily and the northern part of the Messina Straits (Fig. 4). This domain has

Table 2
Estimation of slip by using scarp offset measured on extracted bathymetric profiles (Fig. 7).

Bathy-profiles	Point 1 position: longitude and depth [m]	Point 2 position: longitude and depth [m]	Scarp offset [m]	Estimated erosion (14.5%) [m]	Estimated slip [m]
P1	p55: 16.13938° − 119.19	p52: 16.13972° − 120.64	1.4	0.2	1.2
P2	p54: 16.13188° − 131.51	p35: 16.13378° − 134.71	3.2	0.5	2.7
P3	P44: 16.12818° − 137.61	P28: 16.12911° − 140.62	3.0	0.4	2.6
P4	p45: 16.1222° − 146.88	p36: 16.1231° − 149.99	3.1	0.4	2.7
P5	p45: 16.11758° − 156.48	p36: 16.11879° − 159.68	3.2	0.5	2.7
P6	p41: 16.11378° − 166.72	p37: 16.11432° − 168.33	1.6	0.2	1.4
P7	p34: 16.10838° − 182.41	p29: 16.10898° − 186.08	3.7	0.5	3.1
P8	p50: 16.10019° − 209.61	p49: 16.10039° − 219.89	2.4	0.3	2.1
P9	p54: 16.0946° − 257.52	p53: 16.09479° − 260.41	2.9	0.4	2.5
P10	p44: 16.08819° − 317,81	p43: 16.08839° − 319.99	2.4	0.4	2.1
Average estimated slip [m]					2.3

been discretized with a regular finite-differences grid having uniform resolution of 150 m. Further, we calculated the water inundation along the inner part of the Sant'Eufemia Gulf that needs high-resolution computational grids, which in turn need high-resolution topography and bathymetry. A 10-m resolution topographic database, made available for this study by the University of Calabria (see the above paragraph), is limited to the northern part of the gulf. This database allowed to build a 30-m resolution finite-differences grid to be used in the UBO-TSUFD simulation, and the chosen domain is large enough to contain entirely the fault source. We note that the choice of 30 m is driven by the need to harmonize data of different resolutions, namely the cited 10-m topography inside a limited domain, the 90-m SRTM topography (Jarvis et al., 2008) in the rest of the domain and the 30-m bathymetry made available by the ISTEGE project (Loreto et al., 2013). Inundation is simulated by solving the non-linear version of the shallow-water equations implemented in UBO-TSUFD, and taking advantage of an algorithm that tracks the instantaneous shoreline position at any time step and consequently moves the coastal boundary depending on the instantaneous and local values of the water elevation and of the discharge fluxes.

5.2. KF scenarios technique

The scenario technique is a method of calculating parametric scenarios on MCS intensities (Pettenati and Sirovich, 2006; Sirovich and Pettenati, 2009). The core of the method is the *KF* kinematic function (Sirovich 1996, 1997), which has been applied extensively in the inversion of regional pattern of intensity values (Gentile et al., 2004, Pettenati and Sirovich, 2007) to retrieve information of historical earthquakes. *KF* formula considers the body-wave radiation in an elastic half-space, from a line source within a distance range of approximately 10 to 100 km from the source. It uses 11 parameters: the hypocentral coordinates (latitude, longitude, depth), the fault-plane solution (strike, dip, rake), the shear-wave velocity (Vs), the rupture velocity Vr along strike and antistrike, the seismic moment (M_0) and the percentage of the total rupture length (L). L is calibrated on M_0, through the empirical relationship of Wells and Coppersmith (1994: p.990, Table 2A; "Slip type" = "All," "subsurface rupture length"). The radiation pattern is then converted into pseudo-intensity pattern by an empirical relation, calibrated on five Californian instrumental events and nine Hellenic earthquakes (see equations (2) in Sirovich and Pettenati (2009), and Pettenati and Sirovich (2007)), that allows to transform KF values in modified Mercalli intensities (MMI). The data-fitting function uses 1720 intensity data and it is scaled by moment M_0. We point out that, although the relation is calibrated on MMI, the intensities in this work are in MCS scale. However, the uncertainties brought in this problem by these scale differences are less important than uncertainties intrinsically due to other factors. In support of this, it is worth mentioning the authoritative opinion of Musson et al. (2010): «Ideally, direct conversion between *I* scales should never be made» but, «*I* values are likely to vary more between two seismologists using the same scale than between two scales used by the same seismologist», and thus the relationship between different intensity scales is more or less 1:1.

Finally, in the scenario computation, *KF* is used in the forward model treating the source uncertainties parametrically. Note that *KF* does not consider site amplification.

5.3. Assessing environmental effects

The effect of earthquakes on the environment on land can be split mainly in two categories: slope instability due to additional seismic load and effects due to fluid mobilization, including liquefaction. These studies reveal that the minimum magnitude to induce landsliding is about Mw 5-5.5, (see e.g. Hancox, et al., 1997; Hancox et al., 2002 for New Zealand), that in terms of seismic Intensities can be converted to events having MCS Intensity V (Keefer, 1984). These earthquakes can trigger coherent or disrupted landslides, lateral spread and flow up to 100 km distance from the causative fault plane (Rodríguez et al., 1999). Slope failures and liquefaction reach the greatest expression with larger events. An example is the 1999 Mw 7.6 Chi-Chi earthquake in Taiwan that triggered > 13,000 landslides (Lee, 2013).

According to the above literature, to identify the areas more exposed to environmental effects we, firstly, evaluated the maximum distance from the fault within which these effects may occur, applying the approach to the historical data of the 1905 earthquake (see Fig. 3). Secondly, we analyzed the land characteristics and morphology within the region of potential damage, to identify the areas where landslides (depending on the soil type and slope steepness) or liquefaction (depending on soil type and flatness) may occur.

6. Results

After we defined the most reliable fault geometry and data input (see Section 4.3), the tsunami wave propagation and KF-scenario were modelled using the new input parameters.

6.1. Tsunami wave propagation modelling

Fig. 8 shows snapshots of the tsunami wave propagation in the first 30 min after the earthquake onset. The coseismic displacement, computed by means of the Okada (1992) analytical formulas, induces a strong subsidence of the inner part of the Sant'Eufemia Gulf, while a less pronounced uplift affects the northwestern end of the Gulf as well as the entire area of Capo Vaticano. The general offshore propagation pattern exhibits a first positive front followed by a slightly stronger negative wave. The snapshot taken at 5 min already shows a clear focussing of energy towards the north, which is confirmed by the snapshots taken at later times. The propagation inside the Sant'Eufemia Gulf is rather complicated, due to the peculiar geometry of the Gulf itself and of the bathymetry. A significant portion of tsunami energy is still observable inside the Gulf after 20 min, while at 30 min the main fronts appear to

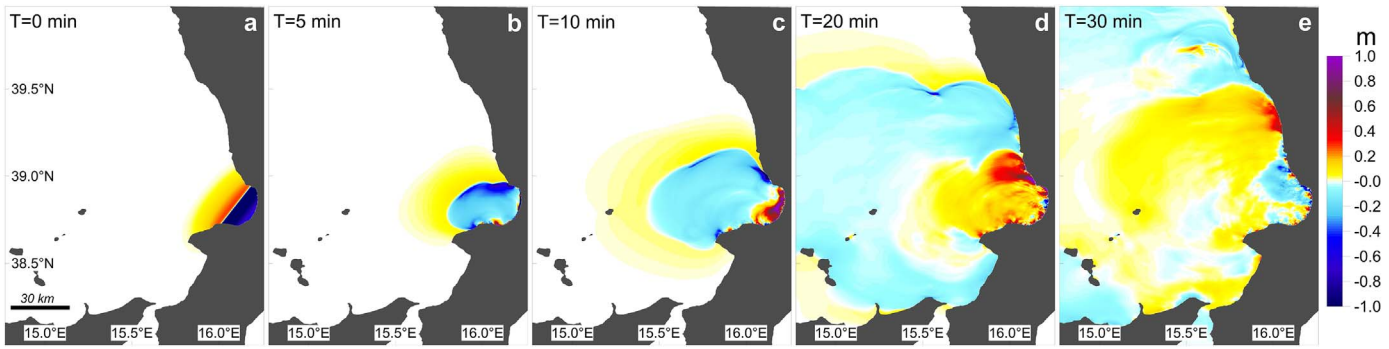

Fig. 8. Snapshots of the tsunami propagation over the chosen computational domain.

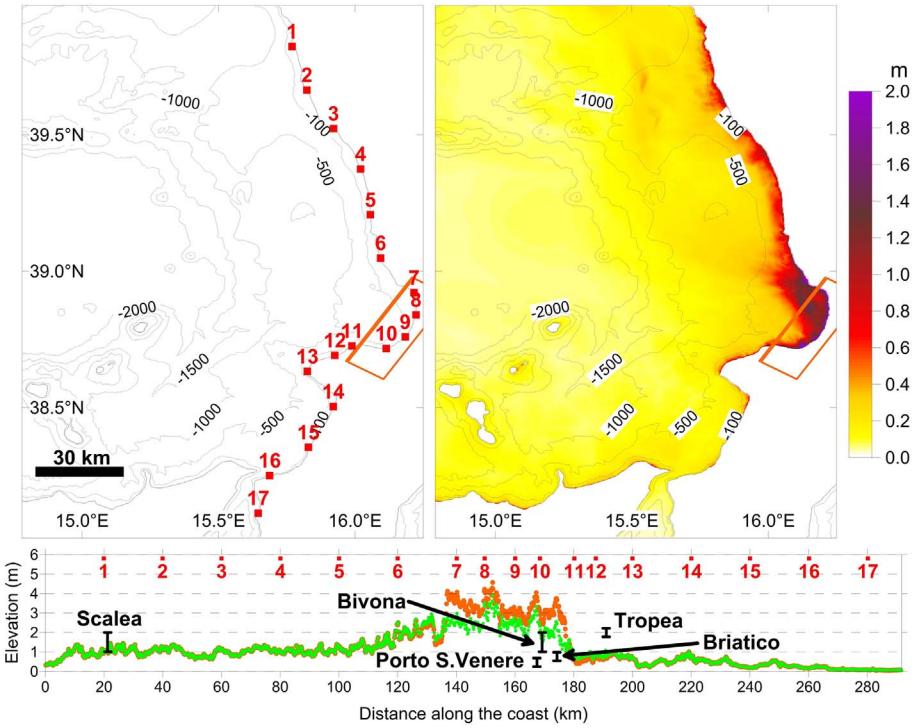

Fig. 9. Upper left: computational domain for linear simulation with contour lines of bathymetry. Red numbered squares indicate some reference coastal points with an approximately 20-km distance from each other, except in the Bivona area where points have a higher density. The orange rectangle represents the surface projection of the fault plane. Upper right: field of maximum water elevation. Bottom: maximum water elevation calculated on the offshore grid nodes closest to the coastline. The orange dots show the maximum elevations corrected for the coseismic displacement, the green dots the maximum elevation without coseismic correction. (For interpretation of the references to colour in this figure legend, the reader is referred to the web version of this article.)

be travelling to the north along the coastline. Only a smaller, but still significant amount of energy propagates towards the south, hitting the Calabria coasts south of Capo Vaticano, the Aeolian islands, the northeastern coasts of Sicily and penetrating also inside the Messina Straits. As regards the tsunami lead time, we may state that the largest inundations in the Sant'Eufemia Gulf are expected within the first 20–25 min after the earthquake, while it will take more than half an hour for the tsunami to produce effects on coastlines located at increasingly larger distances to the north and to the south.

The upper right panel of Fig. 9 shows the pattern of the maximum wave elevation field. The main considerations on the energy distribution introduced above are confirmed here. Indeed, the main concentration of energy is found inside the gulf and especially in its central-northern sector, with maximum elevations exceeding 1 m. The maximum wave impact is more pronounced along the coastlines to the north of the source region. Moreover, due to bathymetry effects, the elevation field shows diffused local maxima also offshore. On the opposite, south of CVP the maximum elevations are lower and typically concentrated in a narrow strip along the coasts.

In the lower panel of Fig. 9 we compared the maximum tsunami elevations with the available observations for the 1905 tsunami (Table 1). In black we indicate the places where observations on tsunami run-up and/or inundation distances are available and the measures themselves, completed with an error bar that is intended to account for the uncertainty related to the conversion from inundation distances to run-up values, as well as to the possible availability of more than one observation for the same location. Recalling the remarks we made on the maximum reported run-up value at Scalea (6 m mentioned only in one account), we decided to attribute a larger reliability to the observed 30-m inundation distance that, laid upon the present-day long, wide and low-lying beach, is compatible with a much more conservative run-up range of 1–2 m. The computed water elevations are shown in two distinct curves, one corresponding to the results as they are produced by the simulation code (green dots), the other taking into account a post-processing correction related to the coseismic displacement effect (orange dots). The main effect of the coseismic correction is to increase the elevations in grid points that experience coseismic subsidence and to decreasing them in points that are co-seismically uplifted.

As expected, the resulting trend exhibits a region of maximum between the northern end of the Sant'Eufemia Gulf and the locality of Briatico to the south; furthermore, an average value of 1 m is foreseen to the north of the source area, while to the south the maximum expected elevation is typically lower. The observation at Scalea remains slightly larger than our computed result, but the discrepancy can be judged reasonable, due to the intrinsic uncertainty on the observed value itself. Three of the available observations are concentrated in the southern part of the gulf (Bivona, Porto Santa Venere, Briatico): with the exception of Bivona, our computed curve tends to overestimate the available observations in this sector, the overestimation being more evident for the coseismically-corrected elevations. Only approximately 15 km to the south, the observed run-up in Tropea is almost two times larger than the computed maximum elevation. This might be partly justified by the fact that we are considering uniform-slip on a fault with no depth-dependent shape, which is only a crude approximation of what happens in realistic faulting.

6.2. *KF scenarios modelling*

Starting from the geometrical model performed in Sandron et al. (2015) and integrating it with new data (see above), the *KF* scenarios have been performed. All the parameters used are listed in Table 3 with their range of variability. The resulting number of source models is 2025, three for each intensity value recorded at the time (Fig. 10a) and that take in account a variable dip value of the fault. We computed the average value of the intensities calculated for each site of the observed intensity database (Fig. 10a). To contour our results, we used our version of Natural Neighbour bivariate interpolation method "*n-n*",

Table 3
Input parameters of the SEF used to perform KF-scenario analysis. Some parameters are derived following Loreto et al. (2012, 2013).

Parameters	Lower limit	Upper limit	Step
Longitude [°] E	15.98	16.14	0.04
Latitude [°] N	38.78	38.05	0.03
Strike [°]	27	39	3
Dip [°] E	45	55	5
Rake [°]	270 fixed		
H [km]	5	9	2
Vs [km/s]	3.6		
Mach	0.8		
Seismic moment [N m] (10^{19})	2.55	4.55	1
L [km]	40		

which is based on the Voronoi tessellation (Sirovich et al., 2002). In this method the "*n-n*" isolines are determined in a unique way, without input parameters, and filters. In other words, they strictly honour the data.

The derived Intensity distribution (Fig. 10b) shows a typical butterfly pattern centered in the Sant'Eufemia Gulf, with highest values in the north, around Gizzeria, and in the south around Tropea-Briatico. These two areas show Intensity values of X MCS. The comparison against observed MCS reveal a better agreement in the far field, while in the near field differences can reach maximum values of − 1.5 and 1.5 on the eastern part (Fig. 10c). The general trend of the Intensity map is well constrained by the observed MCS Intensities and thus trustable, while the misfit of values might be attributed to the conversion law (see method paragraph "KF scenarios technique") and to local effects as discussed in Sandron et al. (2015).

7. Discussion

In the previous sections we showed results of tsunami inundation and of intensity computations and compare them with the available historical data. Here we consider and discuss the potential damage to coastal and inner structures and environment.

7.1. Tsunami flooding

We produced and analyzed inundation maps, describing the spatial pattern of horizontal wave penetration and maximum wave elevation (or maximum water-column height inland). In Fig. 11a, data confirms what was above commented regarding the maximum tsunami energy distribution that is larger and more spatially spread in the northern sector of the Sant'Eufemia Gulf. Nonetheless, the increased grid resolution allows to appreciate the presence of local maxima especially in the southern sector of the Gulf, namely in the areas of Pizzo and Briatico villages, mainly due to the local coastline configuration. Taking in account this fact, we limit the discussion to the domain covered by the 10-m topo-bathymetry. Fig. 11b shows the spatial distribution of the inland water-column height. As a general observation, the water elevation at the coastline rarely exceeds 1.5–2 m, and the water column vanishes over a horizontal distance with variable width but never larger than 660 m. To the north, the inundated area comprises small portions of inhabited areas (Gizzeria Lido, Marinella, Cafarone) and especially the touristic facilities along the beaches. Moving to the south, the density of inhabited settlements decreases significantly south of Ianipari, and inundation regards the long beaches and the adjacent pinewoods, seldom extending to cultivated fields and greenhouses. Among the structures visible through satellite imagery and foreseen to be inundated by our model we cite the former SIR industrial pier and a touristic resort close to the southern end of our 10-m resolution domain. The results presented here could be used in a future tsunami vulnerability analysis for the Tyrrhenian coasts of Calabria, following for instance the methodology recently discussed by Pagnoni et al. (2015) and Pagnoni and Tinti (2016), and applied respectively to the towns of Alexandria (Egypt) and of Siracusa (south-eastern Sicily).

7.2. Onland earthquake effects

The damage distribution assessment is performed by using the derived MCS intensity data (Fig. 10b) overlapped on Google Earth image (Fig. 11c). Accordingly, the CVP and the area around Gizzeria are exposed to the highest damage (X MCS intensity). It follows that a future event similar to the 1905 one would trigger numerous collapses mainly in these two areas, where the risk increases considering the several villages (> 70) and thus the high population density (Fig. 12b; http://demo.istat.it/). This hypothesis well agree with the seismic risk analysis of Italy performed by Lucantoni et al. (2001), in which the central-western Calabria is exposed to the highest risk level due to the high people number that could be involved by house collapses per municipalities. It is worth noting that the coastal strip area from Tropea to Gizzeria (Fig. 11c), is characterized by the presence of numerous villages and touristic/economic activities, such as hotels, resorts, beach infrastructures and the Lamezia airport that continue to expand. All this area is exposed to high damage varying in a range of IX – X MCS.

To make a rough estimate of what a X MCS intensity would produce nowadays in terms of victims and damage, one could make a parallel with the data available from the recent seismic sequence occurred in

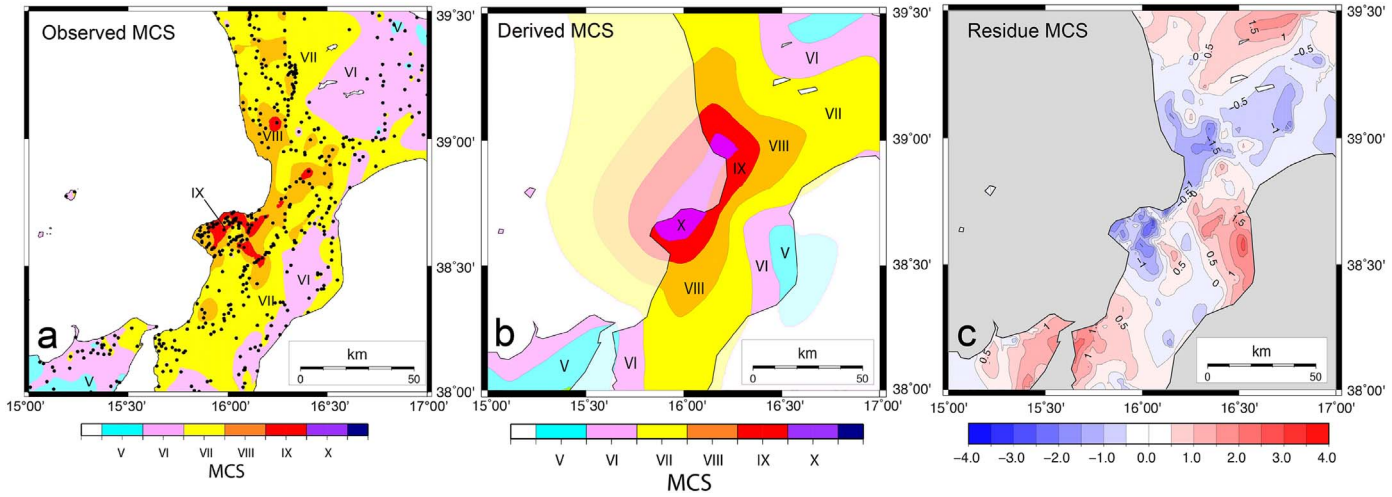

Fig. 10. a) Intensity map of the 1905 Calabria earthquake. All data points location used to produce map contours are plotted as black dots. b) MCS data derived by KF modelling. c) MCS data residuals obtained subtracting the computed values from the observed intensities.

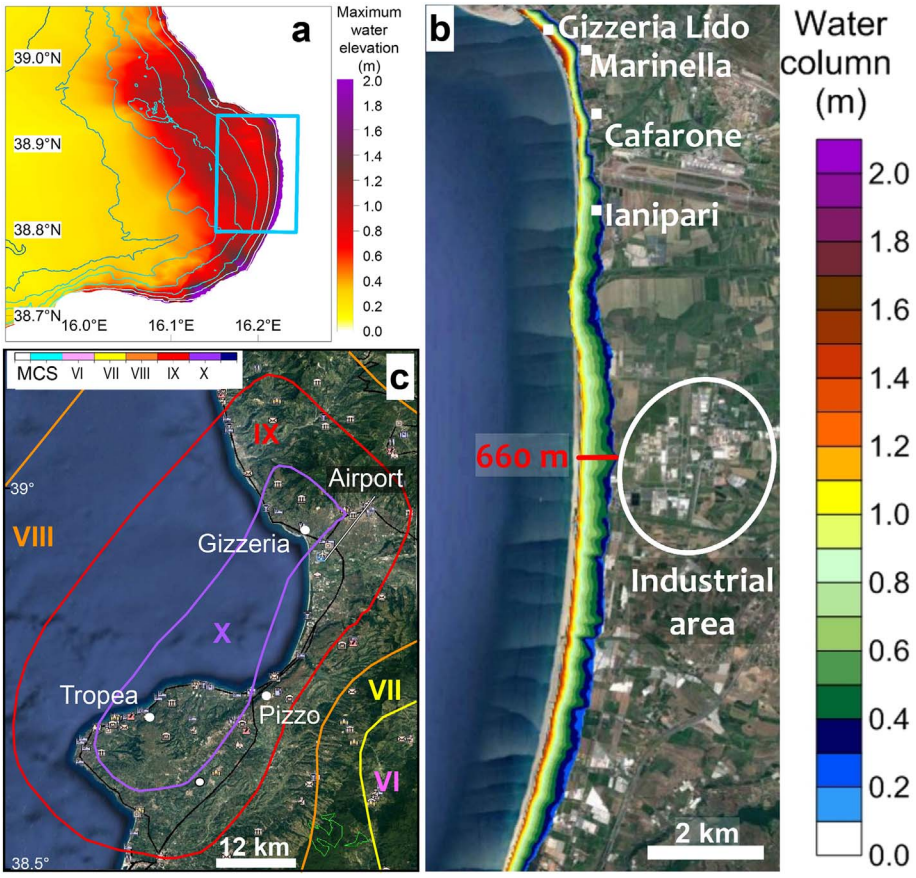

Fig. 11. a) Computational domain covered by the 30-m resolution grid used to study inundation in the northern sector of the Sant'Eufemia Gulf. The cyan-bordered rectangle indicates the area over which 10-m resolution topo-bathymetry is available. b) Result of the inundation modelling in terms of water-column height inland, limited to the above-mentioned sub-domain (Google Earth image). c) Damage distribution map on a Google Earth image. (For interpretation of the references to colour in this figure legend, the reader is referred to the web version of this article.)

the central Apennines in 2016–2017. The first significant earthquake (Mw = 6.2) of the sequence, occurred on 24 August 2016, had an epicentral intensity of X MCS (e.g. Galli et al., 2016): 299 people died and 388 were injured, the area of the most relevant damage included 62 municipalities, a damage cost around 7 bn€ was estimated and the social and economic fabric of the area was dramatically torn, with effects that may take several years to be recovered.

7.3. Environmental impact

The analysis of the impact of the 1905 earthquake on the environment is based on the observations (effects distribution in Fig. 3), and on the estimate of the potential impact. The scatterplot of the environmental effects distribution (Fig. 12 top) shows a logarithmic fall of occurrence underlining hydraulic effects and slope instabilities occurred within 130 km and 110 km, respectively, from the fault center, with the highest occurrence rate being found within the respective distances of 40 km and 35 km. This provides us the area of potential environmental damage and completes the first step of the analysis. The distribution of the effects can be influenced by soil lithology, such as the presence of hard rocks or soft soil, and by morphology, as the presence of gentle (dip $< 2^{\circ}$) or steep (dip $> 15^{\circ}$) slopes. The soil type information (Fig. 3b) suggests that most of the coherent or/and disrupted slides occurred in correspondence of type A and type B soils, while hydraulic phenomena have a looser correlation with the soil type and were observed also in correspondence of tight and loose deposits (soil types C and D; Fig. 3a) that are abundant in alluvial plains.

Consistently with the historical data, we can identify 7 areas most prone to liquefaction occurrence in case of a repetition of the 1905 earthquake, since they have gentle slope (dip $< 2^{\circ}$), and correspond to the main alluvial plains (Fig. 12a). In particular, these are the Gioia Tauro, the Lamezia and Sibari plains, the Crati valley, the Catanzaro System, the Sila inner and Crotone surroundings. Notice that the Lamezia plain (LP) and northern part of the Gioia Tauro plain (GTP) will suffer most, since they are very close to the fault. Joining this feature with the tsunami inundation modelling (Fig. 11b), the Lamezia plain where the airport and others villages and infrastructures are present will be highly exposed to liquefaction and flooding.

With similar reasoning, one can establish that instability phenomena can occur in 5 main areas (Fig. 12b). These are areas having slopes steeper than 15° like the Serre System fault, the Coastal Range, the Sila horst, the Aspromonte region, and, though less evident, the SE-VV system cutting the CVP. According to the historical accounts (Fig. 3b), slope instabilities occurred in steep-side and V-shaped rivers valley, frequently converging in a larger one. This is noticeable in the CVP between Briatico and Vibo Valentia (Figs. 3b and 12b; Chiodo and Sorriso-Valvo, 2006). The highest instability risk is confined to two areas: the southern part of the Coastal Range and the northern part of CVP (thick red squares; Fig. 12b), that happen to be comprised within the 35 km circle around the fault plane center.

Coherently with historical data, the highest risk level is assigned to the zone SE-VVs as deduced by combining our models and impact analysis with the population density computation, ca. 359,02 people per km2 estimated for this zone using data provided by ISTAT and updated to 1th January 2016 (http://demo.istat.it/). A further consideration is that, even if the Vibo Marina city does not fall within the zone SE-VVs, this city can be considered at a high risk level since it is on the beach and therefore exposed to tsunami inundation and also

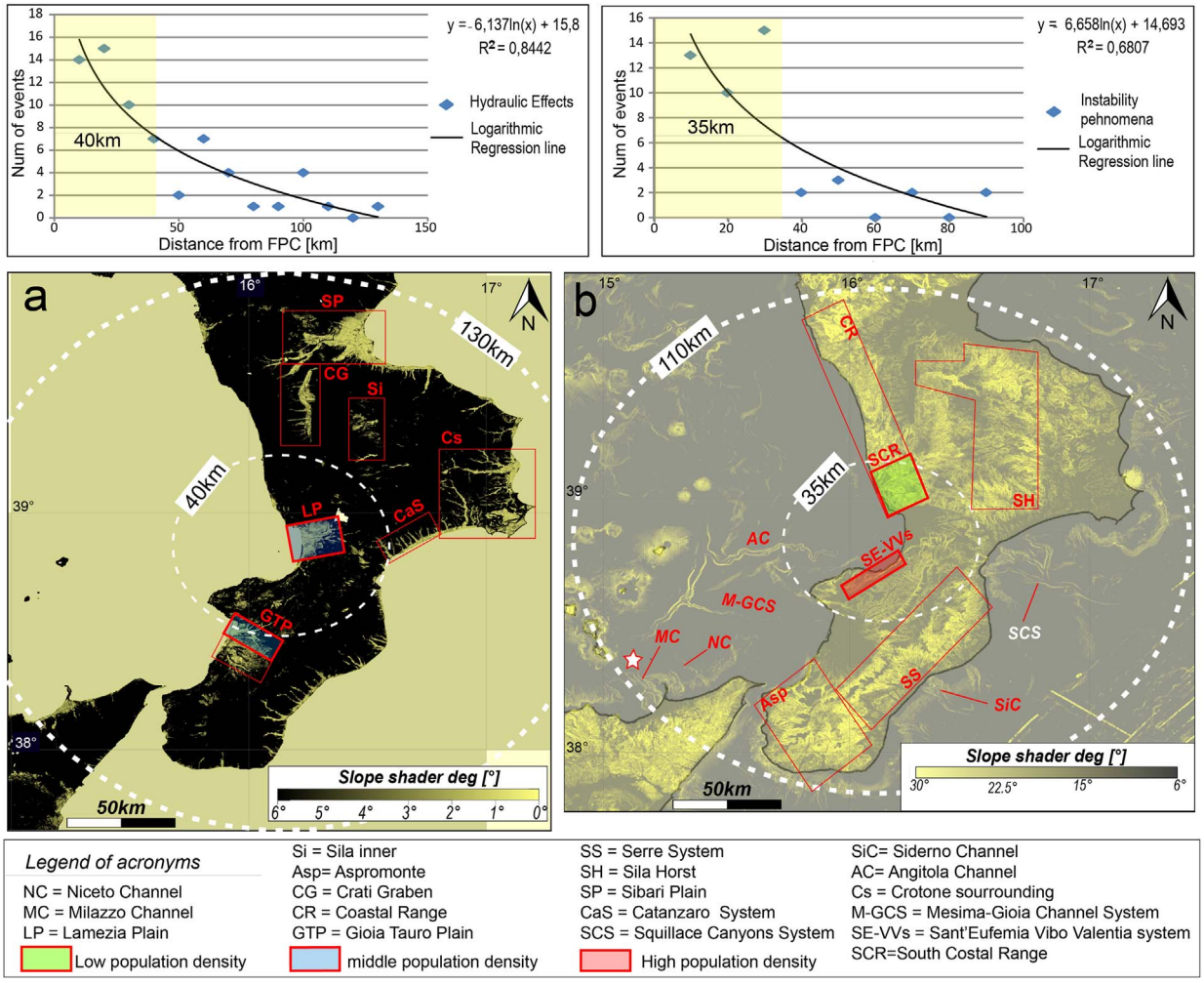

Fig. 12. Maps of slope gradient used to perform a first environmental impact analysis. Onland data are ALOS World 3D-30 m data (http://www.eorc.jaxa.jp/, © JAXA); offshore data are downloaded from EMODnet bathymetry portal (http://portal.emodnet-bathymetry.eu/gebco-bathymetry-basemap) and gridded using GMT software. FPC stands for Fault Place Center. a) Map of hydraulic phenomena impact areas. Above, logarithmic plot of the 1905 earthquake hydraulic effects. b) Map of instability phenomena impact areas. The white star marks the breaking point of the telegraphic cable. Above, logarithmic plot of the 1905 instability phenomena. Population density is estimated using inhabitants number counted from ISTAT website, updated to 1th January 2016 (http://demo.istat.it/), that fall within the analyzed areas. (For interpretation of the references to color in this figure legend, the reader is referred to the web version of this article.)

because it is downstream of the zone interested by collapses. Instead, the zone SCR is less exposed to risk since it has a lower density population (ca. 98,53 people per km2).

7.4. Effects offshore

Offshore, the analysis of the 1905 earthquake effects is more difficult due to very poor historical observations except for the Lipari-Milazzo cable break (Platania, 1907), located (white star; Fig. 12a) at the intersection of the Milazzo and Niceto channels. This element suggests that the 1905 earthquake was able to trigger a turbidity current about 110 km far from the epicentre. Consistently, we can suppose that further catastrophic turbidity currents were triggered along other channels flowing down to the Stromboli valley, such as the Messina-Gioia channel system or the Angitola channel (Fig. 12b), which in modern era deserve more consideration due to the increase of submarine infrastructures.

8. Conclusions

In this study we elaborated an integrated scenario for the 1905 Calabria earthquake. The main results of our analysis can be summarized as follows.

- By combining onland structural and morphological data with offshore geophysical data, we have estimated that the SEF has an approximate length of 40 km, which increases the previous estimate of 25 km (Loreto et al., 2013), and an average co-seismic slip for the 1905 earthquake of 2.3 m. The new length has been used to estimate the fault width, i.e. ca. 17 km, and the earthquake magnitude, Mw 6.9 through the Wells and Coppersmith (1994) scale laws. Updated fault geometry and magnitude were used to run tsunami simulations and to compute KF-scenarios.
- The tsunami propagation and flooding scenarios show that waves propagate mainly northward with maximum elevation in the area of the Sant'Eufemia Gulf. The maximum sea penetration, calculated for the Lamezia plain, resulted to be at a 660-m distance from the shoreline. Comparison between tsunami computations and tsunami observations showed that the agreement is quite satisfactory. It is noted that a repetition of the 1905 tsunami would reach several of the most important infrastructures and industrial areas, and all touristic structures along the beaches.
- The distribution of the KF estimated intensities (MCS) agrees well with that recorded during the 1905 earthquake, in terms of trend, further confirming the hypothesis that the SEF is the causative fault of the 1905 earthquake. The areas that would be more damaged by a repetition of this earthquake are located at the onland end of the

fault and along the coast facing the fault.

- Using the 1905 historical data, the area with the strongest hydraulic effects has been estimated to be within a circle of 40 km radius from the fault center, included in the area of potential damage that has a radius of 130 km. Notice that all the most important alluvial plains of the Calabria region fall within the outer circle. As for slope instability, the estimated radius for their occurrence is 110 km, with the strongest effects occurring within 35 km from the fault center. This analysis has allowed us to conclude that a repetition of the 1905 shock would cause diffuse landsliding in at least 5 mountain areas of Calabria, with the Coastal Range and the northern part of the CVP being the most affected, severely increasing the risk in terms of population exposed.
- The main conclusion is that the SEF is a plausible source for the 1905 earthquake and tsunami, since earthquake and tsunami scenarios agree satisfactorily with the historical observations.

As a final remark, it is worth stressing that, if one considers i) that the minimum magnitude to produce environmental adverse effects is Mw ~ 5–5.5 and ii) that, in addition to the SEF, there is a dense population of active faults, cutting the Calabria region (Fig. 2), capable of triggering earthquakes having Mw > 5.5, hence one can conclude that most part of the region exhibits a high potential for environmental impact.

Acknowledgements

This work was developed within the ISTEGE project 2010 (Loreto et al., 2012), supported by the Istituto Nazionale di Oceanografia e di Geofisica Sperimentale (OGS). We also thank Dr. Antonio Palma (ISPRA Institute), Dr. Riccardo D'Epifanio (Istituto Idrografico della Marina, Genova), and Dr. Carlo Zumaglini (Siap + Micros S.r.l., http://www.siapmicros.com/) for the historical material about tidal network they provided us. All maps and seismic data are managed using the Kingdom software (IHS, Global Inc.), while all bathymetric data are gridded using the open source GMT software. This is the ISMAR contribution n.1924.

References

Almeida-Filho, R., Miranda, F.P., 2007. Mega capture of the Rio Negro and formation of the Anavilhanas Archipelago, Central Amazônia, Brazil: evidences in an SRTM digital elevation model. Remote Sens. Environ. 110 (3), 387–392.

Baratta, M., 1906. Il grande terremoto calabro dell'8 settembre 1905. Atti della Società Toscana di Scienze Naturali, Memorie 22.

Barone, A., Baticci, G., Carboni, S., Colantoni, P., Fabbri, A., Lecca, L., Icolich, R., Sartori, R., Scandone, P., Scarteddu, R., Sechi, F., Torelli, L., Trincardi, F., Zitellini, N., 1983. Progetto finalizzato Oceanograifa e Fondi Marini. In: Ambrosetti, P., Bosi, C., Carraro, F., Ciaranfi, N., Panizza, M., Papani, G., Vezzani, L., Zanferrari, A. (Eds.), Neotectonic map of Italy, scale 1: 500,000. Quad. Ric. Sci. CNR, pp. 114.

Bonardi, G., Cavazza, W., Perrone, V., Rossi, S., 2001. Calabria-Peloritani Terrane and Northern Ionian Sea. In: Martini, L.P., Vai, G.B. (Eds.), Anatomy of an Orogen: The Apennines and Adjacent Mediterranean Basins. Kluwer Academic Publication, pp. 287–306.

Brutto, F., 2016. Geological and structural evolution of tectonically active areas of the central Calabrian Arc. PhD thesis, XXVIII cycle Univ. of Calabria.

Brutto, F., Muto, F., Loreto, M.F., De Paola, N., Tripodi, V., Critelli, S., Facchin, L., 2016. The Neogene-Quaternary geodynamic evolution of the central Calabrian Arc: A case study from the western Catanzaro Trough basin. J. Geodyn. http://dx.doi.org/10.1016/j.jog.2016.09.002.

Castello, B., Moro, M., Chiarabba, C., Di Bona, M., Doumaz, F., Selvaggi, G., Amato, A., 2004. Revised magnitudes of relocated Italian earthquakes catalogue (1981–2002): a new seismicity map of Italy. In: XXIII Congresso del Gruppo Nazionale di Geofisica della Terra Solida (GNGTS), 14–16 Dicembre 2004.

Chiarabba, C., Jovane, L., Di Stefano, R., 2005. A new view of Italian seismicity using 20 years of instrumental recordings. Tectonophysics 395 (3–4), 251–268.

Cox, R.T., 1994. Analysis of drainage-basin symmetry as a rapid technique to identify areas of possible Quaternary tilt-block tectonics: an example from the Mississippi Embayment. Geol. Soc. Am. Bull. 106 (5), 571–581.

CSTI 1.0 Working Group, 2001. Catalogo strumentale dei terremoti italiani dal 1981 al 1996, Versione 1.0 ISBN 88-491-1734-5 Clueb Bologna, CD-ROM.

Critelli, S., Muto, F., Perri, F., Tripodi, V., 2017. Interpreting provenance relations from sandstone detrital modes, southern Italy foreland region: Stratigraphic record of the Miocene tectonic evolution. Mar. Pet. Geol. http://dx.doi.org/10.1016/j.marpetgeo.2017.01.026.

Chiodo, G., Sorriso-Valvo, M., 2006. Frane sismo-indotte: casistica e fenomeni innescati dal terremoto dell'8 settembre 1905. In: Guerra, I., Savaglio, A. (Eds.), Aspetti dei rischi naturali in Calabria, 8 Settembre 1905. Università della Calabria, AGM, pp. 207–224.

Di Capua, G., Lanzo, G., Pessina, V., Peppoloni, S., Scasserra, G., 2011. The recording stations of the Italian strong motion network: geological information and site classification. Bull. Earthq. Eng. 9, 1779–1796. http://dx.doi.org/10.1007/s10518-011-9326-7.

Galli, P., Spina, V., Ilardo, I., Naso, G., 2010. Evidence of active tectonics in southern Italy: the Rossano Fault (Calabria). In: Recent Progress on Earthquake Geology. Nova Science Publishers Inc., New York, pp. 49–78.

Galli, P., Peronace, E., Bramerini, F., Castenetto, S., Naso, G., Cassone, F., Pallone, F., 2016. The MCS intensity distribution of the devastating 24 August 2016 earthquake in central Italy (MW 6.2). Ann. Geophys. 59.

Gentile, F., Pettenati, F., Sirovich, L., 2004. Validation of the Automatic Source Inversion of the U. S. Geological Survey Intensities of the Whittier Narrows, 1987 Earthquake. Bull. Seismol. Soc. Am. 94 (5), 1737–1747.

Ghisetti, F., 1979. Evoluzione neotettonica dei principali sistemi di faglie della Calabria centrale. Boll. Soc. Geol. Ital. 98, 387–430.

Gruppo di Lavoro MPS, 2004. Redazione della mappa di pericolosità sismica prevista dall'Ordinanza PCM 3274 del 20 marzo 2003. Rapporto Conclusivo per il Dipartimento della Protezione Civile. INGV, Milano-Roma, pp. 65 Aprile, + 5 appendices, in italian.

Guarnieri, P., 2006. Plio-Quaternary segmentation of the south Tyrrhenian forearc basin. Int. J. Earth Sci. 95 (1), 107–118.

Hancox, G.T., Dellow, G.D., Perrin, N.D., 1997. Earthquake-induced landsliding in New Zealand and implications for MM intensity and seismic hazard assessment. Institute of Geological and Nuclear Sciences.

Hancox, G.T., Perrin, N.D., Dellow, G.D., 2002. Recent studies of historical earthquake-induced landsliding, ground damage, and MM intensity in New Zealand. Bull. N. Z. Soc. Earthq. Eng. 35 (2), 59–95.

Howard, A.D., 1967. Drainage analysis in geologic interpretation: a summation. AAPG Bull. 51 (11), 2246–2259.

Jarvis, A., Reuter, H.I., Nelson, A., Guevara, E., 2008. Hole-filled seamless SRTM data V4, available from the CGIAR-CSI SRTM 90m Database. http://srtm.csi.cgiar.org.

Keefer, D.K., 1984. Landslides caused by earthquakes. Geol. Soc. Am. Bull. 95 (4), 406–421.

Lee, C.T., 2013. Re-evaluation of Factors Controlling Landslides Triggered by the 1999 Chi-Chi Earthquake. In: Ugai, K., Yagi, H., Wakai, A. (Eds.), Earthquake-Induced Landslides. Springer, Berlin Heidelberg, pp. 213–224.

Loreto, M.F., Zgur, F., Facchin, L., Fracassi, U., Pettenati, F., Tomini, I., Burca, M., Diviacco, P., Sauli, C., Cossarini, G., De Vittor, C., Sandron, D., The Explora Team of Technicians, 2012. In search of new imaging for historical earthquakes: a new geophysical survey offshore western Calabria (southern Tyrrhenian Sea, Italy). Boll. Geofis. Teor. Appl. 53, 385–401.

Loreto, M.F., Fracassi, U., Franzo, A., Del Negro, P., Zgur, F., Facchin, L., 2013. Approaching the seismogenic source of the Calabria 8 September 1905 earthquake: new geophysical, geological and biochemical data from the S. Eufemia Gulf (S Italy). Mar. Geol. 343, 62–75. http://dx.doi.org/10.1016/j.margeo.2013.06.016.

Lucantoni, A., Bosi, V., Bramerini, F., De Marco, R., Lo Presti, T., Naso, G., Sabetta, F., 2001. Seismic risk in Italy. Ingegneria Sismica 1 (2001), 5–36 (In Italian).

Malinverno, A., Ryan, W.B.F., 1986. Extension in the Tyrrhenian Sea and shortening in the Apennines as result of arc migration driven by sinking of the lithosphere. Tectonics 5, 227–245.

Maramai, A., Brizuela, B., Graziani, L., 2014. The Euro-Mediterranean Tsunami Catalogue. Ann. Geophys. 57 (4), S0435.

Martini, M., Scarpa, R., 1982. Italian Earthquakes since 1900. Proc. E. Fermi Summer School in Geophysics. Springer-Verlag, Varenna.

Mercalli, G., 1906. Alcuni risultati ottenuti dallo studio del terremoto calabrese dell'8 settembre 1905. Atti dell'Accademia Pontoniana di Napoli 36, 1–9.

Monaco, C., Tortorici, L., 2000. Active faulting in the Calabrian arc and eastern Sicily. J. Geodyn. 29, 407–424.

Musson, R.M., Grünthal, G., Stucchi, M., 2010. The comparison of macroseismic intensity scales. J. Seismol. 14 (2), 413–428.

Okada, Y., 1992. Internal deformation due to shear and tensile faults in a half-space. Bull. Seismol. Soc. Am. 82 (2), 1018–1040.

Pagnoni, G., Armigliato, A., Tinti, S., 2015. Scenario-based assessment of buildings damage and population exposure due to tsunamis for the town of Alexandria, Egypt. Nat. Hazards Earth Syst. Sci. 15, 2669–2695.

Pagnoni, G., Tinti, S., 2016. Application and comparison of tsunami vulnerability and damage models for the town of Siracusa, Sicily, Italy. Pure Appl. Geophys. 173 (12), 3795–3822. http://dx.doi.org/10.1007/s00024-016-1261-8.

Patacca, E., Scandone, P., 2004. The Plio-Pleistocene thrust belt - foredeep system in the Southern Apennines and Sicily (Italy). In: Crescenti, U., D'Offizi, S., Merlini, S., Lacchi, L. (Eds.), Geology of Italy. Soc. Geol. It, Roma, pp. 93–129.

Pepe, F., Bertotti, G., Ferranti, L., Sacchi, M., Collura, A.M., Passaro, S., Sulli, A., 2013. Pattern and rate of post-20 ka vertical tectonic motion around the Capo Vaticano Promontory (W Calabria, Italy) based on offshore geomorphological indicators. Quatern.Int. 30, 14.

Pettenati, F., Sirovich, L., 2007. Validation of the intensity-based source inversions of three destructive California earthquakes. Bull. Seismol. Soc. Am. 97 (5), 1587–1606. http://dx.doi.org/10.1785/0120060169.

Pettenati, F., Sirovich, L., 2006. Two validations of a kinematic approach to calculate seismic hazard scenarios. In: First European Conference on Earthquake Engineering

and Seismology, pp. 123 3-8 September, Geneva, Switzerland. SC-F 1-I, ID-387, Abstact pag.
Platania, G., 1907. I fenomeni in mare durante il terremoto di Calabria del 1905. Società tipografica modenese (in Italian).
Polonia, A., Torelli, L., Mussoni, P., Gasperini, L., Artoni, A., Klaeschen, D., 2011. The Calabrian arc subduction complex in the Ionian Sea: regional architecture, active deformation, and seismic hazard. Tectonics 30 (5). http://dx.doi.org/10.1029/2010TC002821.
Rizzo, G.B., 1906. In: Clausen, C. (Ed.), Sulla velocità di propagazione delle onde sismiche del terremoto della Calabria del giorno 8 Settembre 1905, (46 pp).
Rizzo, G.B., 1907. Contributo allo studio del terremoto della Calabria del giorno 8 settembre 1905, Atti R. Acc. Peloritana XXII, fasc. I. pp. 2–87.
Rodríguez, C.E., Bommer, J.J., Chandler, R.J., 1999. Earthquake-induced landslides: 1980–1997. Soil Dyn. Earthq. Eng. 18 (5), 325–346.
Rosenbaum, G., Gasparon, M., Lucente, F.P., Peccerillo, A., Miller, M.S., 2008. Kinematics of slab tear faults during subduction segmentation and implications for Italian magmatism. Tectonics 27 (2) TC2008. http://dx.doi.org/10.1029/2007TC002143.
Rovida, A., Camassi, R., Gasperini, P., Stucchi, M., 2011. CPTI11, the 2011 Version of the Parametric Catalogue of Italian Earthquakes. Milano, Bologna. http://emidius.mi.ingv.it/CPTI.
Rovida, A., Locati, M., Camassi, R., Lolli, B., Gasperini, P. (Eds.), 2016. CPTI15, the 2015 version of the Parametric Catalogue of Italian Earthquakes. Istituto Nazionale di Geofisica e Vulcanologia. http://dx.doi.org/10.6092/INGV.IT-CPTI15.
Sandron, D., Loreto, M.F., Fracassi, U., Tiber, L., 2015. Shaking scenarios from multiple source models shed light on the Mw 7 Calabria 8 September 1905 earthquake (S Italy). Bull. Seismol. Soc. Am. 105 (2A), 912–927.
Sirovich, L., Pettenati, F., 2009. Validation of a kinematic and parametric approach to calculating intensity scenarios. Soil Dyn. Earthq. Eng. 29 (7), 1113–1122. http://dx.doi.org/10.1016/j.soildyn.2008.12.007.
Sirovich, L., 1996. A simple algorithm for tracing out synthetic isoseismals. Bull. Seismol. Soc. Am. 86, 1019–1027.
Sirovich, L., 1997. Synthetic isoseismals of three earthquakes in California and Nevada. Soil Dyn. Earthq. Eng. 16 (6), 353–362.
Sirovich, L., Musson, R.M., Pettenati, F., Cavallini, F., Bobbio, M., 2002. Natural-neighbor Isoseismals. Bull. Seismol. Soc. Am. 92 (5), 1933–1940.
Slejko, D., Peruzza, L., Rebez, A., 1998. Seismic hazard maps of Italy. Ann. Geophys. 41 (2). http://hdl.handle.net/2122/1436.
Tertulliani, A., Cucci, L., 2009. Clues to the identification of a seismogenic source from environmental effects. The case of the 1905 Calabria (southern Italy) earthquake. Nat. Hazards Earth Syst. Sci. 9, 1787–1803. http://dx.doi.org/10.5194/nhess-9-1787-2009.
Tansi, C., Muto, F., Critelli, S., Iovine, G., 2007. Neogene-Quaternary strike-slip tectonics in the central Calabrian Arc (southern Italy). J. Geodyn. 43, 393–414.
Tinti, S., 1993. Evaluation of Tsunami Hazard in Calabria and Eastern Sicily, Italy. Springer, Netherlands, pp. 141–157.
Tinti, S., Gavagni, I., 1995. A smoothing algorithm to enhance finite-element tsunami modelling: an application to the 5 February 1783 calabrian case, Italy. Nat. Hazards 12 (2), 161–197. http://dx.doi.org/10.1007/BF00613075.
Tinti, S., Maramai, A., 1996. Catalogue of tsunamis generated in Italy and in Côte d'Azur, France: a step towards a unified catalogue of tsunamis in Europe. Ann. Geophys. 39 (6), 1253–1299.
Tinti, S., Piatanesi, A., 2002. Numerical simulations of the 8 September 1905 Calabrian tsunami (southern Italy) as a tool to improve the assessment of tsunami risk on the Calabrian coast. In: ITS 2001 Proceedings, pp. 4–5.
Tinti, S., Armigliato, A., 2001. Impact of large tsunamis in the Messina Straits, Italy: the case of the 28 December 1908 tsunami. In: Hebenstreit, G.T. (Ed.), Tsunami Research at the End of a Critical Decade. vol. 18. Springer, Netherlands, pp. 139–162.
Tinti, S., Armigliato, A., Bortolucci, E., 2001. Contribution of tsunami data analysis to constrain the seismic source: the case of the 1693 eastern Sicily earthquake. J. Seismol. 5, 41–61.
Tinti, S., Armigliato, A., 2003. The use of scenarios to evaluate the tsunami impact in southern Italy. Mar. Geol. 199 (3), 221–243.
Tinti, S., Maramai, A., Graziani, L., 2004. The new catalogue of Italian tsunamis. Nat. Hazards 33 (3), 439–465.
Tinti, S., Tonini, R., 2013. The UBO-TSUFD tsunami inundation model: validation and application to a tsunami case study focused on the city of Catania, Italy. Nat. Hazards Earth Syst. Sci. 13, 1795–1816. http://dx.doi.org/10.5194/nhess-13-1795-2013.
Tortorici, L., Monaco, C., Tansi, C., Cocina, O., 1995. Recent and active tectonics in the Calabrian arc (Southern Italy). Tectonophysics 243 (1), 37–55.
Tortorici, G., Bianca, M., De Guidi, G., Monaco, C., Tortorici, L., 2003. Fault activity and marine terracing in the Capo Vaticano area (southern Calabria) during the Middle-Late Quaternary. Quat. Int. 101/102, 269–278. http://dx.doi.org/10.1016/S1040-6182(02)00107-6.
Tripodi, V., Muto, F., Critelli, S., 2013. Structural style and tectono-stratigraphic evolution of the Neogene Quaternary Siderno basin, southern Calabrian Arc, Italy. Int. Geol. Rev. 55, 468–481.
Valensise, G., Pantosti, D., 2001. Seismogenic faulting, moment release patterns and seismic hazard along the central and southern Apennines and the Calabrian arc. In: Vai, G.B., Martini, I.P. (Eds.), Anatomy of an Orogen: The Apennines and Adjacent Mediterranean Basins. Kluwer Academic Publishers, Dordrecht, pp. 495–512.
Van Dijk, J.P., Scheepers, P.J.J., 1995. Neotectonic rotations in the Calabrian Arc; implications for a Pliocene-Recent geodynamic scenario for the Central Mediterranean. Earth Sci. Rev. 39, 207–246.
Wells, D., Coppersmith, K., 1994. New empirical relationship among magnitude, rupture length, rupture width, rupture area and surface displacement. Bull. Seismol. Soc. Am. 84, 974–1002.
Westaway, R., 1993. Quaternary uplift of southern Italy. J. Geophys. Res. 98 (B12), 741–772.
Zecchin, M., Praeg, D., Ceramicola, S., Muto, F., 2015. Onshore to offshore correlation of regional unconformities in the Plio-Pleistocene sedimentary successions of the Calabrian Arc (central Mediterranean). Earth Sci. Rev. 142, 60–78.